

RESEARCH LETTER

10.1002/2015GL064746

Key Points:

- The LADEE neutral mass spectrometer detected exospheric ions at the Moon
- NMS detected H_2^+ , He^+ , C^+ , Ne^+ , Na^+ , K^+ , Ar^+ , and an ambiguous 28 amu ion
- Simultaneous plasma data are critical for interpreting NMS ion measurements

Correspondence to:

J. S. Halekas,
jasper-halekas@uiowa.edu

Citation:

Halekas, J. S., M. Benna, P. R. Mahaffy, R. C. Elphic, A. R. Poppe, and G. T. Delory (2015), Detections of lunar exospheric ions by the LADEE neutral mass spectrometer, *Geophys. Res. Lett.*, 42, doi:10.1002/2015GL064746.

Received 29 MAY 2015

Accepted 17 JUN 2015

Accepted article online 19 JUN 2015

Detections of lunar exospheric ions by the LADEE neutral mass spectrometer

J. S. Halekas¹, M. Benna^{2,3}, P. R. Mahaffy², R. C. Elphic⁴, A. R. Poppe⁵, and G. T. Delory^{4,5}

¹Department of Physics and Astronomy, University of Iowa, Iowa City, Iowa, USA, ²NASA Goddard Space Flight Center, Greenbelt, Maryland, USA, ³CSST, University of Maryland, Baltimore County, Baltimore, Maryland, USA, ⁴NASA Ames Research Center, Mountain View, California, USA, ⁵Space Sciences Laboratory, University of California, Berkeley, California, USA

Abstract The Lunar Atmosphere and Dust Environment Explorer (LADEE) Neutral Mass Spectrometer (NMS), operating in ion mode, provides sensitive detections of ions from the lunar exosphere. By analyzing ion-mode data from the entire mission, utilizing Acceleration, Reconnection, Turbulence, and Electrodynamics of the Moon's Interaction with the Sun (ARTEMIS) plasma and magnetic field measurements to organize NMS data and eliminate background sources, we identify highly significant detections of lunar ions at mass per charge of 2, 4, 12, 20, 28, 39, and 40, moderately significant detections at 14 and 23, and weak detections at 24, 25, and 36. Unlike many previous observations of Moon-derived ions, an outward pointing viewing geometry ensures that these ions originate from the exosphere, rather than directly from the surface. For species with known neutral distributions, inferred ion production rates appear consistent with expectations for both magnitude and spatial distribution, assuming photoionization as the predominant source mechanism. Unexpected signals at mass per charge 12 and 28 suggest the presence of a significant exospheric population of carbon-bearing molecules.

1. Introduction and Context

The lunar exosphere has been a subject of active study since the Apollo era and remains a rich subject because of the diversity of processes that provide its sources and sinks, including micrometeorite bombardment, charged-particle sputtering, photostimulated desorption, and eventual ionization and pickup by the flowing plasma. The tenuous nature of the exosphere has made measuring its structure and composition an ongoing challenge, and only upper limits exist for many species [Stern, 1999; Cook *et al.*, 2013].

The recently completed Lunar Atmosphere and Dust Environment Explorer (LADEE) mission [Elphic *et al.*, 2014] included the Neutral Mass Spectrometer (NMS) [Mahaffy *et al.*, 2014]. The NMS operates by electron-impact-ionizing exospheric gases and mass resolving them with unit mass resolution using a quadrupole mass filter, but can also operate in a nonionizing mode to detect ambient ions. Benna *et al.* [2015] have described NMS measurements of the noble gases He, Ne, and Ar in neutral form. In this paper we present first results and detections from NMS ion-mode measurements.

As described by Hartle and Killen [2006], ion measurements provide a highly sensitive diagnostic of planetary exospheres. Ion composition measurements typically have lower background than neutral composition measurements and thus enable detections of tenuous species, including metallic ions with high photoionization rates. Several previous missions have detected lunar pickup ions, including Active Magnetospheric Particle Tracer Explorers and Wind at distant locations [Hilchenbach *et al.*, 1991; Mall *et al.*, 1998], Chang'E [Wang *et al.*, 2011], Kaguya [Saito *et al.*, 2010; Yokota *et al.*, 2009; Tanaka *et al.*, 2009], and ARTEMIS [Halekas *et al.*, 2012, 2013; Poppe *et al.*, 2012] from lunar orbit. These missions detected a variety of ions, including species tentatively identified as H_2^+ , He^+ , C^+ , O^+ , Na^+ , Al^+ , Si^+ , K^+ , Ar^+ , Ca^+ , and Fe^+ , with some uncertainty due to multiple species located near masses of 27–28 and 39–40 amu. Other than Kaguya, previous missions could not have distinguished ions produced by ionization of exospheric components and those produced directly by sputtering [Elphic *et al.*, 1991].

2. NMS Ion-Mode Measurements

The LADEE NMS instrument has two apertures, a closed source and an open source [Mahaffy *et al.*, 2014]. The open source, used to measure species that would react with surfaces, has a narrow field of view with a Gaussian response with $\sim 5^\circ$ full width at half maximum. By turning off the filament used to electron-impact

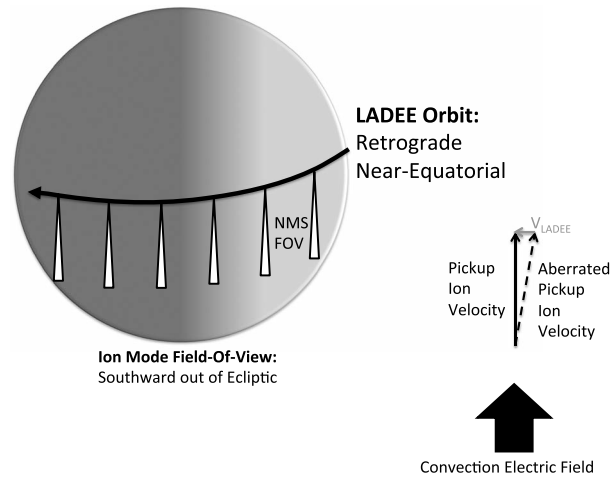


Figure 1. Schematic illustration of the LADEE NMS observing geometry, showing the retrograde near-equatorial orbit, the NMS ion-mode field of view, and a diagram showing the apparent velocity of a newborn pickup ion in the spacecraft frame, including the aberration due to spacecraft motion.

ionized gas, one can utilize the open source to detect ambient ions with energies from near thermal up to ~25 eV, with roughly uniform sensitivity. Given the constrained energy and angular response, one expects to measure newly born ions produced within a few tens of kilometers from the spacecraft, at times when the convection electric field points into the NMS aperture.

As shown in Figure 1, to maximize the chance of detecting exospheric ions, LADEE reoriented during ion scans so that the NMS aperture pointed south. Given the orbit of LADEE, this places the surface out of the field of view and provides a good chance that the convection electric field (northward for a $-B_x/+B_y$ Parker spiral magnetic field) points into the aperture. By excluding the surface, we can say with confidence that observed ions, which given their large gyroradii, travel almost directly along the electric field in the

NMS energy range [Halekas et al., 2012, 2013], must result from ionization of the exosphere, rather than sputtering of ions from the surface. During the LADEE mission, NMS operated in ion mode 79 times, with each scan lasting from shortly prenoon to midnight local time, covering 19 preselected mass per charge channels.

NMS did not observe ions from the densest portion of the exosphere, since it responds to a column that extends southward from the spacecraft, with a density that decreases as a function of altitude. Given the constrained energy range that NMS responded to, one can predict an inverse dependence of measured flux on convection electric field strength. The expected count rate C measured by NMS for a perfectly aligned electric field E , given an aperture size A , detection efficiency F , an upper energy cutoff W_c (~25 eV) and a production rate $q(l)$ along the column extending antiparallel to the electric field, scales as follows:

$$C = A \times F \times \int_0^{W_c/E} q(l) dl \tag{1}$$

Given a uniform production rate, one would measure a flux proportional to W_c/E . In reality, the production rate $q(l)$, the product of ionization rate R and neutral density $n(l)$, varies along the column. The neutral density falls exponentially with altitude, with a scale height related to the mass and the energetics of the processes that released particles from the surface. For light and/or energetic particles, the scale height does not play a significant role, but for heavy particles, the scale height is comparable to the column length.

An additional complication results from the aberration caused by the spacecraft motion, which shifts the apparent velocity of freshly produced ions, causing them to arrive from a slight angle with respect to the electric field, as shown in Figure 1. This velocity aberration affects heavier ions to a greater degree, since they have a smaller velocity at a given energy. Sensitivity decreases rapidly for velocities not perfectly aligned with the boresight, given the narrow angular acceptance. Spacecraft charging may also affect the response, by shifting the energy band pass and thus the portion of the column sampled.

Figure 2 shows four NMS ion scans, all from the quiet-time solar wind. We utilized data from ARTEMIS [Angelopoulos, 2010] to determine the motional electric field of the flowing plasma, computing it from the magnetic field [Auster et al., 2008] and the plasma velocity [McFadden et al., 2008] and shifting it by the solar wind propagation time to the Moon (for typical solar wind speeds, <60 s). We utilize an average value from both probes, excluding data from the wake.

These four ion scans have representative characteristics, showing a scattering of counts throughout (mainly detector dark counts), but higher count rates when the electric field points into the NMS aperture in sunlight (enabling photoionization or solar wind charge exchange ionization of neutral gases). We typically observe

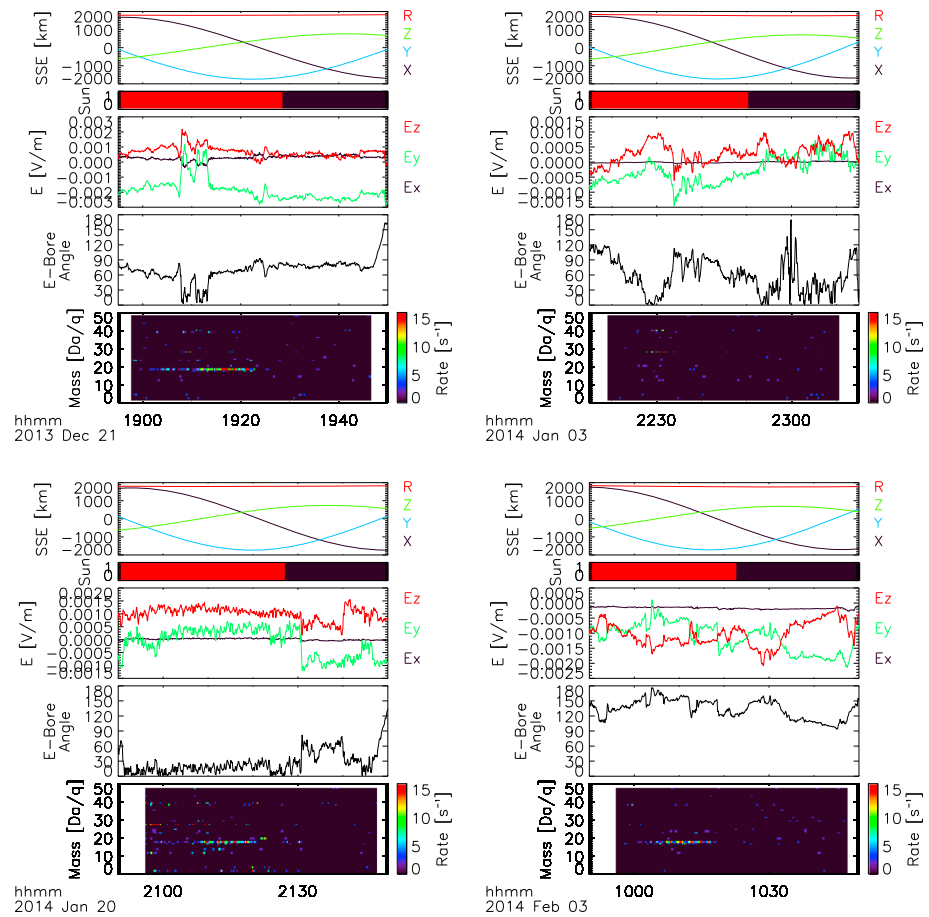


Figure 2. Results from four representative NMS ion-mode runs in the quiet-time solar wind, showing the LADEE position in Selenocentric Solar Ecliptic (SSE) coordinates, Sun/shadow status, the motional electric field (also in SSE) derived from ARTEMIS measurements of plasma flow velocity and magnetic field and propagated to the Moon, the E-Bore angle between the NMS boresight and the anti-electric-field direction, and count rates measured as a function of time and mass by NMS.

the highest count rates at mass per charge 28 and 40, and these appear well organized by the electric field, though small Alfvénic fluctuations in the solar wind make it difficult to resolve the angle between the electric field and the boresight to better than a few tens of degrees.

We also observed sporadic high count rates at the water group mass per charge channels 17 and 18 but found that these counts appear for any electric field direction, implying that they do not result from acceleration of newly born ions along the electric field. Count rates for water group ions correlate strongly with the solar wind density from ARTEMIS. We cannot determine the production mechanism but suspect solar wind sputtering and/or solar wind charge exchange with neutral vapor from the spacecraft. Neither of these should produce a bulk flux directed into the NMS aperture; however, measurements from Rosetta have indicated a significant self-scattered component in the spacecraft neutral coma, which could explain some particle velocities directed into the aperture [Schlappi et al., 2010]. Negative spacecraft charging could also explain the acceleration of newborn ions into the aperture; however, this appears unlikely given basic expectations of current balance. Regardless, we exclude water group ions from subsequent analyses.

3. NMS Ion Detections

While individual ion scans provide us with an idea of the characteristics of the measurements, given the rather low count rates, we prefer to look at ensemble averages to address the question of detectability. We utilize a subset of the data to obtain the best signal. Since very energetic particles can penetrate the sensor housing and interact directly with the detectors, we first utilize ARTEMIS electrostatic analyzer data

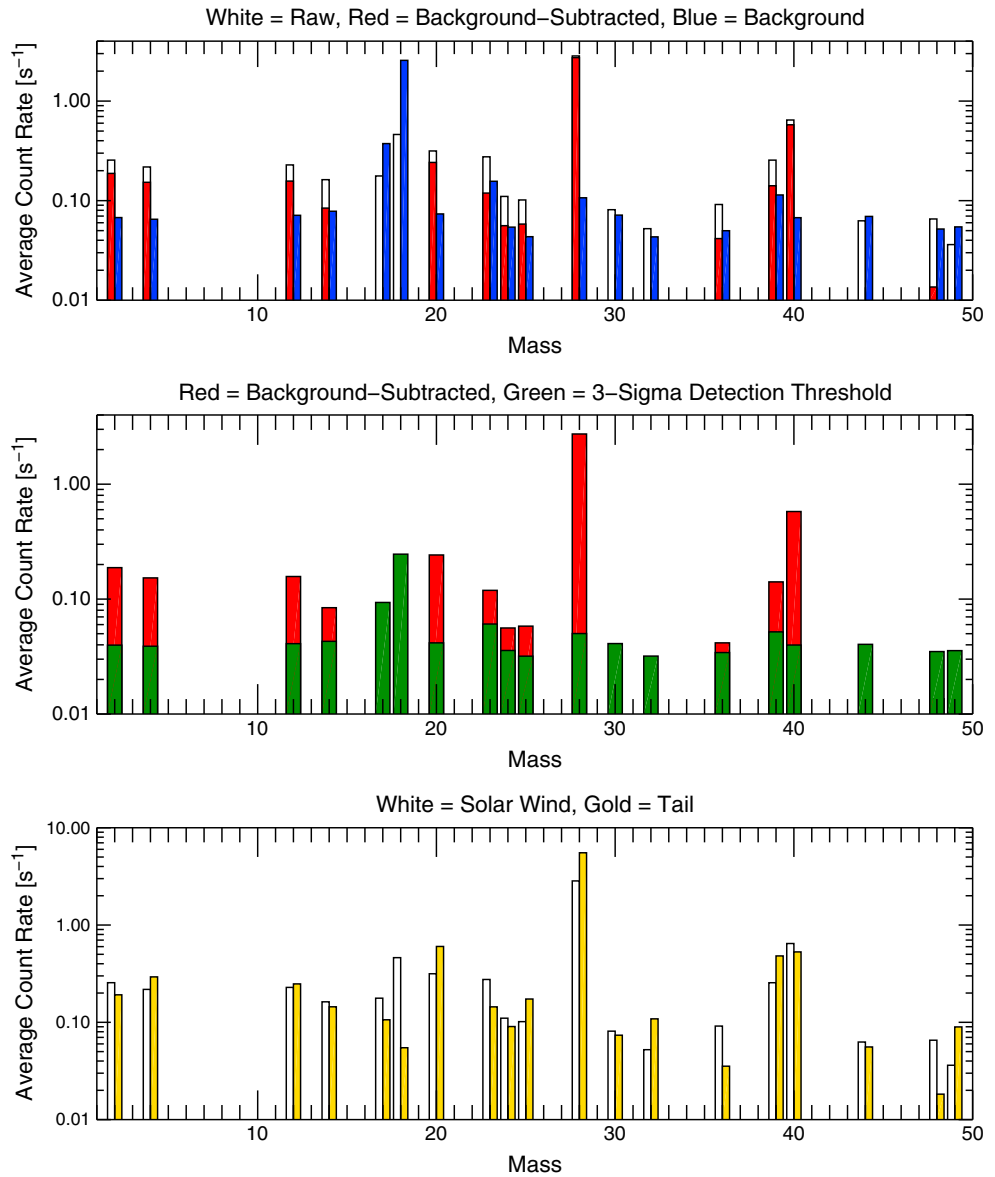


Figure 3. (top) Dayside mission-averaged count rates for all measured mass per charge channels during quiet-time solar wind intervals with the E-Bore angle between the anti-electric-field direction and the NMS boresight less than 45°, the mission-averaged background rate derived from quiet-time solar wind measurements with E-Bore angle greater than 90°, and the background-subtracted rate consisting of the difference between these two. (middle) The background-subtracted rate as compared to a 3 sigma detection criteria based on the mission-averaged background rate. (bottom) Comparison of mission-averaged dayside count rates from the quiet-time solar wind to those from the terrestrial magnetosphere, both for times with the E-Bore angle less than 45°.

to eliminate solar energetic particle events and identify quiet-time solar wind intervals with no penetrating background. We select a subset of those times when the spacecraft was within 120° of the subsolar point (thus plausibly responding to a column of newly born ions from the exosphere) and when the electric field derived from ARTEMIS pointed within 45° of the antiboresight direction (a wide angular range in order to account for magnetic fluctuations in the solar wind).

A background rate for the NMS detector chain of ~0.133 counts per second was estimated during instrument integration and testing [Mahaffy et al., 2014]. During flight, we determined a more accurate mass-dependent instrument background by performing the same selection as above but picking times when the electric field derived from ARTEMIS pointed at an angle greater than 90° from the antiboresight direction. Given the

background rate B thus defined and the total measurement time T , we computed background-subtracted rates and the 3 sigma minimum detectable activity $3\sqrt{B/T}$ [Knoll, 2010]. We show the raw and background-subtracted rates, along with background rates and detection thresholds, in Figure 3. We found background rates for most mass per charge channels of about half of the ground-estimated value, indicating good detector performance and low background. We again note a significant background for the water group ions 17 and 18 (with the latter higher than real count rates at any mass per charge except 28). We also note slightly enhanced backgrounds at mass per charge 23, 28, and 39, possibly indicating a contribution from a spacecraft-generated source. In these three channels, the background-subtracted rate still exceeded the detection threshold.

After subtracting the mass-dependent background, we obtained high signal (>5 sigma) detections at mass per charge 2, 4, 12, 20, 28, 39, and 40, moderately significant (~ 5 sigma) detections at mass per charge 14 and 23, and weak detections at mass per charge 24, 25, and 36 (>3 sigma, but <5 sigma). These detections appear plausible given previous neutral and ion measurements, which have identified species at or near almost all these mass groups. The large count rates for mass per charge 28 provided the greatest surprise, given that of the candidate species (N_2^+ , CO^+ , and Si^+), the first two have relatively low photoionization yields [Huebner *et al.*, 1992] and the third has a very low upper limit on neutral abundance [Flynn and Stern, 1996; Cook *et al.*, 2013]. CO^+ appears the most plausible, possibly indicating significant exospheric populations of carbon-bearing molecules, as hypothesized by Hodges [1976].

We also compared solar wind data to a smaller data set from the Earth's magnetotail in Figure 3. Despite greater uncertainty in the electric field derived from ARTEMIS (resulting from both small-scale structure and low plasma flow speeds), magnetotail data selected by electric field direction show a fairly similar pattern to solar wind data, except for a clear reduction in the water group signal (which correlates with plasma density and thus decreases in the magnetotail). For the same column-averaged production rates, one might expect to see higher count rates in the tail, given lower electric field strengths, but data do not obviously bear out this expectation. On the other hand, the farther the measured column extends, the lower the production rate for a typical exospheric distribution, so the ratio between counts in the tail to those in the solar wind should be smaller than the ratio of electric field, particularly for heavier species. Furthermore, for small plasma flows, low-energy ions no longer all come from the same direction, and gyration becomes significant even at low energies. Finally, in a low-density environment like the tail, the spacecraft potential should increase to large positive values, shifting the effective energy range NMS responds to and effectively pushing the column observed by NMS farther from the spacecraft (to higher altitude). These competing factors are difficult to determine quantitatively and leave the question of whether neutral densities differ between the solar wind and magnetotail unresolved.

4. Local Time Dependence of Ion Flux

For solar wind time periods, there are enough counts to bin data as a function of position. Figure 4 (top row) shows the signal and background count rates for eight mass per charge channels, as a function of angle from the subsolar point. For the most part, background remains constant as a function of sun angle, but background rates for mass per charge 23, 28, and 39 do rise very slightly on the dayside, hinting at a spacecraft contribution (background for 17 and 18, not shown, also peaks on the dayside). Figure 4 (middle left) shows background-subtracted rates, indicating detectable signals on the dayside and few detectable signals in shadow, consistent with photoionization and/or charge exchange with the solar wind.

In order to convert measured count rates from NMS into a measure of ion production rates, we developed a kinematic model that utilizes the measured electric field and the energy and mass-dependent aberration due to the spacecraft velocity to compute the expected ion fluxes as a function of energy and angle for a given ion production rate. By convolving these fluxes with the energy and angular response of NMS in ion mode, the physical size of the aperture, and the efficiency of detectors and electronics, we can then compute an expected ion count rate for a given production rate. For each observation, this model takes into account the instantaneous LADEE position, orientation, and velocity, and the angle between the electric field propagated from ARTEMIS and the boresight, to compute an effective sensitivity in units of count rate/production rate [$s^{-1}/(cm^{-3} s^{-1}) = cm^3$] for the entire measured column (the length of which depends on the magnitude of the electric field), assuming uniform production rate over that column.

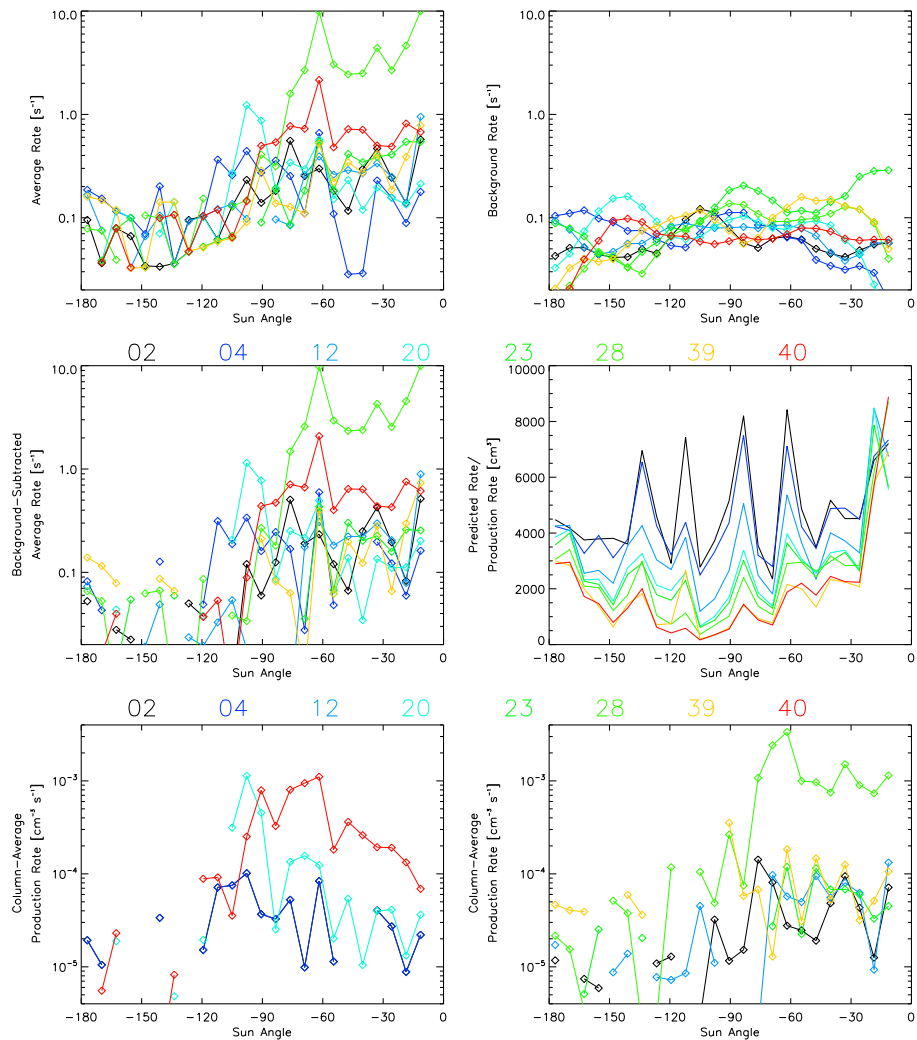


Figure 4. (top left) Mission-averaged count rates in the quiet-time solar wind as a function of the angle from the subsolar point of the spacecraft position, for all times with the E-Bore angle $< 45^\circ$. (top right) Background rates derived from solar wind times with the anti-electric-field direction greater than 90° from the NMS boresight. (middle left) Background-subtracted rates formed by subtracting the quantities in the previous two panels. (middle right) The predicted count rate per unit ion production rate. (bottom) An estimate of column-averaged ion production rates, computed by dividing the background-subtracted rates by the predicted count rate per unit production rate, for (left) noble gas ions and (right) other species.

One could relax the assumption of uniform production rate, but this would require imposing assumptions about the scale height of the neutral parent species.

Since the response of NMS in ion mode depends sensitively on the angle between the electric field and the boresight, it proves difficult to utilize model results to analyze individual observations. Instead, we compute an ensemble average for all quiet-time solar wind observations. Figure 4 (middle right) shows the resulting predicted sensitivity, as a function of Sun angle, for eight ion masses. We note several features in the resulting curves that require some explanation. Large fluctuations in predicted sensitivity for all masses result from a small number of time periods with good electric field alignment and small electric field magnitudes (leading to large predicted sensitivity). The broad depression in predicted sensitivity near the terminator, particularly apparent for heavy species, results from the aberration due to the velocity of the spacecraft (see Figure 1). Since the convection electric field (a cross product between the magnetic field and the plasma flow, with the latter almost entirely in the X direction) has almost no X component, even a V_x component of a few km/s significantly reduces the fraction of time with the electric field optimally aligned with the narrow aperture, leading to significant undersampling of heavy ion fluxes near the terminator.

By dividing background-subtracted rates by relative sensitivity, we derived column-averaged production rates from NMS data. We emphasize that, given the ensemble-averaged nature of the predicted sensitivity, these curves can only represent approximate ion production rates and only then under the assumption of uniform production over the entire column measured by NMS. For light and/or energetic ions, the latter assumption is typically safe, but for heavy ions, the actual production rate close to the spacecraft may significantly exceed the column average, with the production rate from farther away correspondingly lower.

Despite the necessarily approximate nature of our calculations, derived production rates appear reasonable for most species. For example, given dayside neutral argon densities at LADEE altitude of $\sim 5000 \text{ cm}^{-3}$ [Benna *et al.*, 2015] and quiet-Sun photoionization rates on the order of $3 \times 10^{-7} \text{ s}^{-1}$ [Huebner *et al.*, 1992], one expects ion production rates on the order of $1.5 \times 10^{-3} \text{ cm}^{-3} \text{ s}^{-1}$, in agreement with our results. Encouragingly, inferred local time distributions also appear reasonable for all three noble gas ions (He^+ , Ne^+ , and Ar^+), with peak count rates near the terminator and declining count rates toward the subsolar point, consistent with a convolution of ionization sources with known neutral densities [Benna *et al.*, 2015].

Ions of mass per charge 2, 12, 23, and 39, presumably corresponding to H_2^+ , C^+ , Na^+ , and K^+ , appear widespread across the dayside, with slightly higher production rates near the terminator, but more uniform production rates than the noble gas ions, consistent with lighter and/or more energetic neutral populations broadly distributed around the Moon. The presence of counts in shadow may indicate real ions produced by charge exchange in the wake, but given their low level, we refrain from drawing conclusions from these points.

An unidentified ion species at mass per charge 28 has the highest derived production rates. We note that though somewhat surprising, this appears consistent with Wind, which found significant fluxes in this mass range (these were ascribed to surface-derived Al^+ and Si^+ at that time) [Mall *et al.*, 1998]. CO^+ provides the most plausible candidate to explain 28 amu ions from an exospheric source, with a subsolar neutral surface density upper limit of $\sim 14,000 \text{ cm}^{-3}$ [Feldman and Morrison, 1991] (limits from Lunar Reconnaissance Orbiter place a more stringent limit just behind the terminator of 700 cm^{-3} [Cook *et al.*, 2013]). Given a photoionization rate of $4 \times 10^{-7} \text{ s}^{-1}$, a thermal CO population at the upper limit would lead to production rates at LADEE altitude on the order of $3 \times 10^{-3} \text{ cm}^{-3} \text{ s}^{-1}$, comparable to our results. A nonthermal release mechanism or a significant contribution from other ionization mechanisms could help lower the neutral density needed to explain the observations.

We also obtain a clear detection of C^+ , with the production rate seemingly implying a significant neutral density. Assuming a photoionization rate of $6 \times 10^{-7} \text{ s}^{-1}$, one would infer a neutral density above LADEE altitude on the order of 100 cm^{-3} . This would appear surprising, given optical limits on the subsolar surface density of 200 cm^{-3} [Feldman and Morrison, 1991] and a limit near the terminator of 1.6 cm^{-3} [Cook *et al.*, 2013]. However, the NMS result represents one of several recent detections or inferences of C^+ at significant levels [Tanaka *et al.*, 2009; Yokota *et al.*, 2009; Halekas *et al.*, 2013]. We note that photodissociation of CO should lead not only to C, but also to significant direct production of C^+ , which could explain the large observed C^+ fluxes without violating known neutral density limits for C. Therefore, NMS results suggest the presence of a significant exospheric contribution from carbon-bearing molecules. We do not detect CO_2 , but this would presumably have a smaller scale height, making it more difficult to observe. Unfortunately, NMS ion measurements did not cover mass per charge 16 (due to an unfortunately chosen operational script), the location of a few surprising detections [Mall *et al.*, 1998; Yokota *et al.*, 2009; Tanaka *et al.*, 2009; Halekas *et al.*, 2013], and another possible dissociation byproduct of CO.

5. Implications and Conclusions

Ion mass composition measurements provide a sensitive diagnostic of tenuous exospheres like that of the Moon. Using LADEE NMS ion-mode measurements, supported by plasma and magnetic field data from ARTEMIS, we clearly detected species with mass per charge of 2, 4, 12, 20, 28, 39, and 40 and made moderately significant detections at mass per charge 14, 23, 24, 25, and 36. Simultaneous plasma measurements prove critical in analyzing the ion composition measurements, allowing the organization of measured fluxes and the removal of background. For species with known neutral distributions, the local time dependence and inferred production rates correspond to expectations. Significant counts at

mass per charge 12 and 28 suggest the presence of an important lunar exospheric contribution from carbon-bearing molecules, consistent with predictions [Hodges, 1976]. Further study and detailed modeling are needed to understand how neutral and ion abundances vary with solar wind flux, micrometeorite flux, and lunar phase.

Acknowledgments

We acknowledge support from the LADEE Guest Investigator Program under grant NNX14AR24G and also thank SSERVI for supporting this study. A.R.P. was supported by NASA LASER grant #NNX13AJ97G. We acknowledge NASA contract NAS5-02099 for use of data from ARTEMIS, specifically J.P. McFadden and C.W. Carlson for ESA data and K. H. Glassmeier, U. Auster, and W. Baumjohann for FGM data provided under the lead of the Technical University of Braunschweig and with financial support through the German Ministry for Economy and Technology and the German Center for Aviation and Space (DLR) under contract 50 OC 0302. We acknowledge [http://phidrates.space.swri.edu/Huebner et al.](http://phidrates.space.swri.edu/Huebner) [1992] for photoionization rates. ARTEMIS data are publicly available on NASA's CDAWeb. LADEE data are publicly available through the Planetary Data System.

The Editor thanks two anonymous reviewers for their assistance in evaluating this paper.

References

- Angelopoulos, V. (2010), The ARTEMIS mission, *Space Sci. Rev.*, doi:10.1007/s11214-010-9687-2.
- Auster, H. U., et al. (2008), The THEMIS fluxgate magnetometer, *Space Sci. Rev.*, *141*, 235–264.
- Benna, M., P. R. Mahaffey, J. S. Halekas, R. C. Elphic, and G. T. Delory (2015), Variability of helium, neon, and argon in the lunar exosphere as observed by the LADEE NMS instrument, *Geophys. Res. Lett.*, *42*, 3723–3729, doi:10.1002/2015GL064120.
- Cook, J. C., S. A. Stern, P. D. Feldman, G. R. Gladstone, K. D. Retherford, and C. C. C. Tsang (2013), New upper limits on numerous atmospheric species in the native lunar atmosphere, *Icarus*, *225*, 681–687.
- Elphic, R. C., H. O. Funsten, B. L. Barraclough, D. J. McComas, M. T. Paffett, D. T. Vainan, and G. Heiken (1991), Lunar surface composition and solar wind-induced secondary ion mass spectrometry, *Geophys. Res. Lett.*, *18*, 2165–2168, doi:10.1029/91GL02669.
- Elphic, R. C., et al. (2014), The lunar atmosphere and dust environment explorer mission, *Space Sci. Rev.*, doi:10.1007/s11214-014-0113-z.
- Feldman, P. D., and D. Morrison (1991), The Apollo 17 ultraviolet spectrometer: Lunar atmosphere measurements revisited, *Geophys. Res. Lett.*, *18*, 2105–2109, doi:10.1029/91GL01998.
- Flynn, B. C., and S. A. Stern (1996), A spectroscopic survey of metallic species abundances in the lunar atmosphere, *Icarus*, *124*, 530–536.
- Halekas, J. S., A. R. Poppe, G. T. Delory, M. Sarantos, W. M. Farrell, V. Angelopoulos, and J. P. McFadden (2012), Lunar pickup ions observed by ARTEMIS: Spatial and temporal distribution and constraints on species and source locations, *J. Geophys. Res.*, *117*, E06006, doi:10.1029/2012JE004107.
- Halekas, J. S., A. R. Poppe, G. T. Delory, M. Sarantos, and J. P. McFadden (2013), Using ARTEMIS pickup ion observations to place constraints on the lunar atmosphere, *J. Geophys. Res. Planets*, *118*, 81–88, doi:10.1029/2012JE004292.
- Hartle, R. E., and R. M. Killen (2006), Measuring pickup ions to characterize the surfaces and exospheres of planetary bodies: Applications to the Moon, *Geophys. Res. Lett.*, *33*, L05201, doi:10.1029/2005GL024520.
- Hilchenbach, M., D. Hovestadt, B. Klecker, and E. Mobius (1991), Detection of singly ionized energetic lunar pick-up ions upstream of Earth's bow shock, in *Solar Wind Seven*, edited by E. Marsch and G. Schwenn, pp. 150–155, Pergamon, New York.
- Hodges, R. R., Jr. (1976), The escape of solar-wind carbon from the moon, *Proc. Lunar Sci. Conf.*, *7th*, 493–500.
- Huebner, W. F., J. J. Keady, and S. P. Lyon (1992), Solar photo rates for planetary atmospheres and atmospheric pollutants, *Astrophys. Space Sci.*, *195*, 1–294.
- Knoll, G. (2010), *Radiation Detection and Measurement*, Wiley, New York.
- Mahaffey, P. R., et al. (2014), The neutral mass spectrometer on the lunar atmosphere and dust environment explorer mission, *Space Sci. Rev.*, *185*(1–4), 27–61, doi:10.1007/s11214-014-0043-9.
- Mall, U., E. Kirsch, K. Cierpka, B. Wilken, A. Soding, F. Neubauer, G. Gloeckler, and A. Galvin (1998), Direct observation of lunar pick-up ions near the Moon, *Geophys. Res. Lett.*, *25*, 3799–3802, doi:10.1029/1998GL900003.
- McFadden, J. P., C. W. Carlson, D. Larson, M. Ludlam, R. Abiad, B. Elliott, P. Turin, M. Marckwordt, and V. Angelopoulos (2008), The THEMIS ESA plasma instrument and in-flight calibration, *Space Sci. Rev.*, *141*, 277–302.
- Poppe, A. R., R. Samad, J. S. Halekas, M. Sarantos, G. T. Delory, W. M. Farrell, V. Angelopoulos, and J. P. McFadden (2012), ARTEMIS observations of lunar pickup ions in the terrestrial magnetotail lobes, *Geophys. Res. Lett.*, *39*, L17104, doi:10.1029/2012GL052909.
- Saito, Y., et al. (2010), Inflight performance and initial results of Plasma energy Angle and Composition Experiment (PACE) on SELENE (Kaguya), *Space Sci. Rev.*, *154*, 265.
- Schlappi, B., et al. (2010), Influence of spacecraft outgassing on the exploration of tenuous atmospheres with in situ mass spectrometry, *J. Geophys. Res.*, *115*, A12313, doi:10.1029/2010JA015734.
- Stern, S. A. (1999), The lunar atmosphere: History, status, current problems, and context, *Rev. Geophys.*, *37*, 453–491, doi:10.1029/1999RG900005.
- Tanaka, T., et al. (2009), First in situ observation of the Moon-originating ions in the Earth's magnetosphere by MAP-PACE on SELENE (KAGUYA), *Geophys. Res. Lett.*, *36*, L22106, doi:10.1029/2009GL040682.
- Wang, X. D., et al. (2011), Detection of $m/q = 2$ pickup ions in the plasma environment of the Moon: The trace of exospheric H₂⁺, *Geophys. Res. Lett.*, *38*, L14204, doi:10.1029/2011GL047488.
- Yokota, S., et al. (2009), First direct detection of ions originating from the Moon by MAP-PACE IMA onboard SELENE (KAGUYA), *Geophys. Res. Lett.*, *36*, L11201, doi:10.1029/2009GL038185.